15th World Congress on Computational Mechanics (WCCM-XV)
8th Asian Pacific Congress on Computational Mechanics (APCOM-VIII)
Virtual Congress: 31 July – 5 August 2022
S. Koshizuka (Ed.)

NUMERICAL SIMULATION OF INTERACTION BETWEEN TWO SAVONIUS TURBINES AIMED AT PRACTICAL APPLICATION OF OCEAN CURRENT POWER GENERATION

AKIKO MINAKAWA[1] AND TETUYA KAWAMURA[2]

[1] Ochanomizu University
2-1-1 Otsuka, Bunkyo-ku, Tokyo 112-8610, Japan
minakawa.akiko@is.ocha.ac.jp

[2] The Open University of Japan
3-29-1 Otsuka, Bunkyo-ku, Tokyo 112-0012, Japan
kawamura@is.ocha.ac.jp

Key words: Savonius rotor, ocean current power generation , numerical simulation, Flow field, Interaction between wind turbines

Abstract. *One of the vertical axis wind turbines that utilize drag force is the Savonius wind turbine. Savonius wind turbines are characterized by low speed rotation and high torque, so they are rarely used for wind power generation but have possibility to apply to ocean current power generation, which has been attracting attention recently. In this report, we actually performed a numerical simulation of the flow using suitable grid, focusing mainly on the case where two wind turbines are rotating in reverse at a constant speed, and investigated the state of the flow field. Two-dimensional incompressible Navier-Stokes equations are adopted as the basic equation and solved numerically using the finite difference method. In addition, in order to enable calculation even in a high Reynolds number flow, the nonlinear term of the equations are approximated by using the third-order accuracy upstream difference method. The simulation is performed under the condition that the flow corresponds to three types of angles of 90 degrees, 45 degrees, and 0 degrees with respect to the line connecting the centers of the two wind turbines. The flow field differs greatly depending on each angle, and the interaction between the two wind turbines has been clarified.*

1 INTRODUCTION

Reducing carbon dioxide from fossil fuels, which cause extreme weather and climate change, is an urgent issue. In April 2021, the Japanese government set carbon dioxide emissions in 2030 at 46% of 2013 levels. Since the nuclear safety myth has collapsed due to the accident at the nuclear power plant caused by the Great East Japan Earthquake in 2011, efforts are being made to efficiently obtain renewable energy derived from nature. Among them, wind energy is a representative of renewable energy, and many wind power plants and wind farms are being constructed in various parts of Japan. On the other hand, wind power generation has the disadvantage that it is easily affected by the weather as well as solar power generation. For a stable energy supply, it is important to increase the methods of obtaining

renewable energy so that increase the options. One of them is the use of ocean current energy that can cover the shortcomings of wind power and solar power. Since the energy of a moving fluid is proportional to the density of the fluid, the energy of the seawater flow, which is about 1000 times the density of air, is literally an order of magnitude higher than that of wind power. Furthermore, in Japan, the Kuroshio Current, which is one of the largest currents in the world, flows in the coastal waters, and there are many areas with fast currents. Therefore, it is possible to overcome the disadvantage of wind power generation that there are few places where wind turbines can be constructed in a small land area.

Wind turbines and water turbines are classified into lift type and drag type. The former uses the lift from a fluid flow, and has the characteristic that it can rotate faster than the flow velocity. On the other hand, the torque is small. A typical example is a propeller-type wind turbine installed all over the country. The latter utilizes the drag force, and although it cannot rotate faster than the flow velocity, it is characterized by a large torque. Savonius wind turbines and cross-flow wind turbines are typical examples[1][2]. The rotation speed can be changed using a transmission, but the energy loss is large. Therefore, the propeller type is currently the mainstream for wind power generation, since it is efficient to use a wind turbine that rotates at high speed. On the other hand, the lift type is not suitable because the ocean current has a small flow velocity.

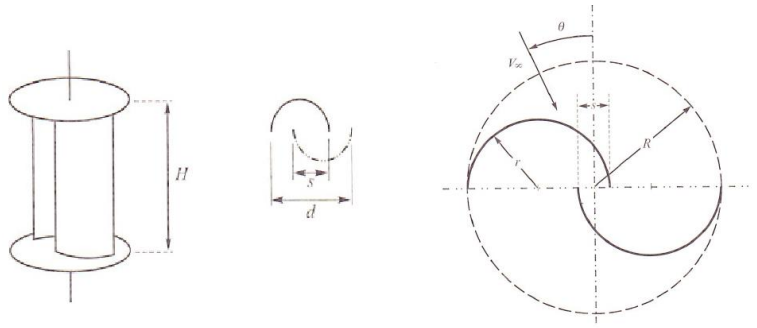

Figure 1: Savonius turbine

.

As shown in Fig.1, the shape of the Savonius wind turbine (rotating device) is that of dividing a hollow cylinder like a drum placed in the vertical direction into two at the surface including the shaft and shifts it laterally so as to have an overlap. This wind turbine is called the Savonius turbine because it was invented by the Finnish engineer Savonius and patented in 1924.

In estimating the performance of a rotating device for power generation, it is indispensable to investigate the flow around the device when it is rotating. Ultimately, even if in the case of making a model and measuring the torque directly, it is efficient to systematically change the shape of the rotating device after fully understanding the flow. Numerical simulation is useful in such cases[3][4][5].

When the Savonius type rotating device is actually installed in the sea, if it is installed alone, a rotational force is applied to the entire device and it is difficult to make it stand still. However, stable installation can be expected because the rotation can be canceled by installing the two devices close to each other and connecting them with a support rod or the like so as to they rotate in opposite directions. Of course, since the two devices interact, it is

important to estimate the effect. Therefore, in this report, we mainly focused on two Savonius-type rotating devices that rotate in the opposite direction, and performed a numerical simulation of the two-dimensional flow in the cross section perpendicular to the wind turbine axis. At this time, it is expected that the flow field will change significantly depending on the angle at which the flow hits the line connecting the two rotating devices. Therefore, as a typical case, the calculation was performed when the flow is parallel to the above line, when it is perpendicular to the line, and when it hits at an angle of 45 degrees. The effect of tip speed ratio on the power coefficient is also investigated.

2 NUMERICAL METHOD

2.1 Grid generation

The usual method of dividing a complex area by a grid system used by the finite difference method is to divide the original area into several smaller areas and join them together, instead of dividing by a single grid system. At this time, it is desirable that the grid points match at the boundary of the region. If it is difficult to match the boundaries, the procedure is to superimpose the two regions so that they overlap and interpolate the physical quantities at one boundary from the physical quantities at the adjacent grid points of the other region. In this case as well, it is desirable that the grid lines in one direction match in both regions in order to improve the accuracy of interpolation.

Another requirement for grids in this research is the ability to properly represent rotating objects. As an effective analysis method for the flow around a rotating object such as a wind turbine, there is a method of expressing the Navier-Stokes equation, which is a basic equation, in a rotating coordinate system that rotates with the object. By doing so, the calculation becomes possible without rotating the grid. However, there are some problems.

One of the most essential problems is that when simulating the situation where many wind turbines are rotating, it cannot be expressed by one rotation system. In such a case, it is necessary to use a different rotating coordinate system for each wind turbine and connect them appropriately. Since the analysis target of this research includes the case of multiple wind turbines, it is desirable to have a grid that is as accurate as possible when joining.

The following grids are proposed in this research as grids that meet these requirements. It is assumed that two Savonius wind turbines are placed close to each other.

(1) The area containing one Savonius wind turbine consists of five partial areas.

(2) These five areas are nested.

(3) The outermost region A has a concave shape with a part missing from the rectangle.

(4) The outer edge of the inner region B has a rectangular shape that exactly fits into the recessed portion of (3).

(5) The inner edge of region B is circular.

(6) The other inner region C has a circular outer edge and a dumbbell-like shape with an inner edge that partially includes the blades of a Savonius wind turbine. The inner edge of the region B and the outer edge of the region C overlap by one grid.

(7) The region D, which has a dumbbell-shaped outer edge, has a shape with the overlap region peculiar to the Savonius wind turbine removed.

(8) The innermost region E is the above overlap region.

The grid system used in this study is shown in Fig.2 and Fig.3.

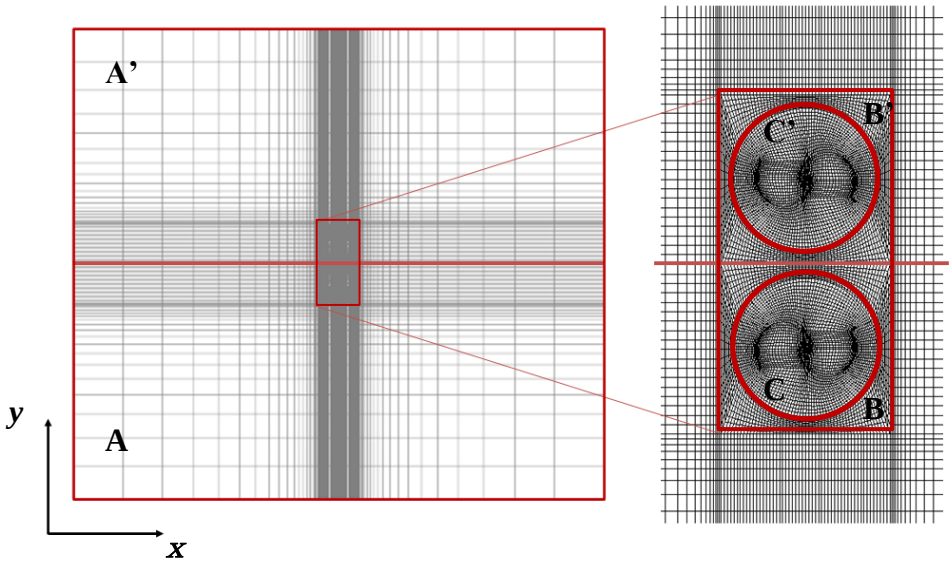

Figure 2: Computational grid for two rotating devices (left: whole, right: near the wind turbine)

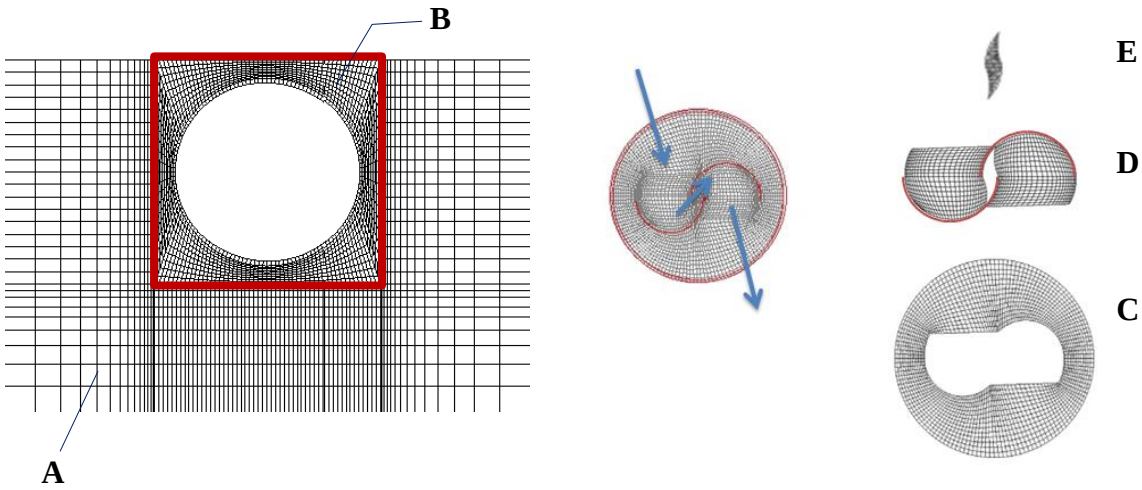

Figure 3 Stationary coordinate system grid (left half) and rotating coordinate system grid (right half)

2.2 Basic Equation

The flow field is governed by the incompressible Navier-Stokes equation because the flow is sufficiently slow compared to the speed of sound. The method used in this report is a method of connecting a stationary coordinate system in the external region (left in Fig.3) and a rotating coordinate system rotating at the same angular velocity as the wind turbine in the internal region (right in Fig.3) with a circular boundary. The basic equation is expressed in two types, a stationary coordinate system and a rotating coordinate system. The basic equations are as follows:

$$\frac{\partial u}{\partial x}+\frac{\partial v}{\partial y}=0 \tag{1}$$

$$\frac{\partial u}{\partial t}+u\frac{\partial u}{\partial x}+v\frac{\partial u}{\partial y}=-\frac{\partial p}{\partial x}+\frac{1}{Re}\left(\frac{\partial^2 u}{\partial x^2}+\frac{\partial^2 u}{\partial y^2}\right) \tag{2}$$

$$\frac{\partial v}{\partial t}+u\frac{\partial v}{\partial x}+v\frac{\partial v}{\partial y}=-\frac{\partial p}{\partial y}+\frac{1}{Re}\left(\frac{\partial^2 v}{\partial x^2}+\frac{\partial^2 v}{\partial y^2}\right) \tag{3}$$

$$\frac{\partial U}{\partial X}+\frac{\partial V}{\partial Y}=0 \tag{4}$$

$$\frac{\partial U}{\partial t}+U\frac{\partial U}{\partial X}+V\frac{\partial U}{\partial Y}-\omega^2 X+2\omega V=-\frac{\partial p}{\partial X}+\frac{1}{Re}\left(\frac{\partial^2 U}{\partial X^2}+\frac{\partial^2 U}{\partial Y^2}\right) \tag{5}$$

$$\frac{\partial V}{\partial t}+U\frac{\partial V}{\partial X}+V\frac{\partial V}{\partial Y}-\omega^2 Y-2\omega U=-\frac{\partial p}{\partial Y}+\frac{1}{Re}\left(\frac{\partial^2 V}{\partial X^2}+\frac{\partial^2 V}{\partial Y^2}\right) \tag{6}$$

The lowercase letters represent the stationary coordinate system and the uppercase letters represent the rotating coordinate system, and the following relationship holds between the two. The relations of position components between them are

$$x=Xcos\theta+Ysin\theta, y=-Xsin\theta+Ycos\theta \tag{7}$$

$$X=xcos\theta-ysin\theta, Y=xsin\theta+ycos\theta \tag{8}$$

where θ is the angle between two coordinate systems. Also, there are following relations of velocity components between them:

$$u=Ucos\theta+Vsin\theta+\omega y, v=-Usin\theta+Vcos\theta-\omega X \tag{9}$$

$$U=ucos\theta-vsin\theta-\omega Y, V=usin\theta+vcos\theta+\omega X \tag{10}$$

Schematic figure of these two coordinate systems is shown in Fig.4.

Figure 4: Coordinate systems

Fractional step method is used to solve basic equation numerically[6]. In order to enable calculation even in a high Reynolds number flow, the nonlinear term of the equations are approximated by using the third-order accuracy upstream difference method[7].

The boundary conditions were set to uniform flow for velocity on the inflow side, normal derivative 0 for pressure, atmospheric pressure for pressure on the outflow side, and normal

derivative 0 for velocity.

Since the outside of the inner region and the inside of the outer region are circumferential and overlap by one grid, the velocity and pressure of the grid points are calculated for each time step by one-dimensional interpolation in the circumferential direction. The tip speed ratio of the wind turbine (= tip velocity /uniform flow velocity) is changed from 0.2 to 1.5, and the flow is 90 degrees (angle of attack 0 degrees), 45 degrees (angle of attack 45 degrees), and 0 degrees (angle of attack 90 degrees) with respect to the line connecting the center of the wind turbine. The Reynolds number was set to 20000 in consideration of the resolution of the grid.

3 RESULTS AND DISCUSSIONS

3.1 Flow field

Fig.5 shows the flow field near the blade of the lower rotating device by a velocity vector when the angle of attack is 0 degrees. In the Savonius type rotating device, there is a gap between the two blades, and a part of the flow received by the windward blade flows into it and pushes the leeward blade. Therefore, the structure of the turbine is such that the torque is larger than when there is no gap.

Looking at Fig.5, it can be seen that the flow is certainly flowing into the gap.

The flow is strongest in the case of (b) tilted by 45 degrees with respect to the flow, while in the case of 0 degrees indicated by (a) and (f), a vortex is generated in the gap portion. Because it obstructs the inflow into the gap, the flow in the gap is almost gone.

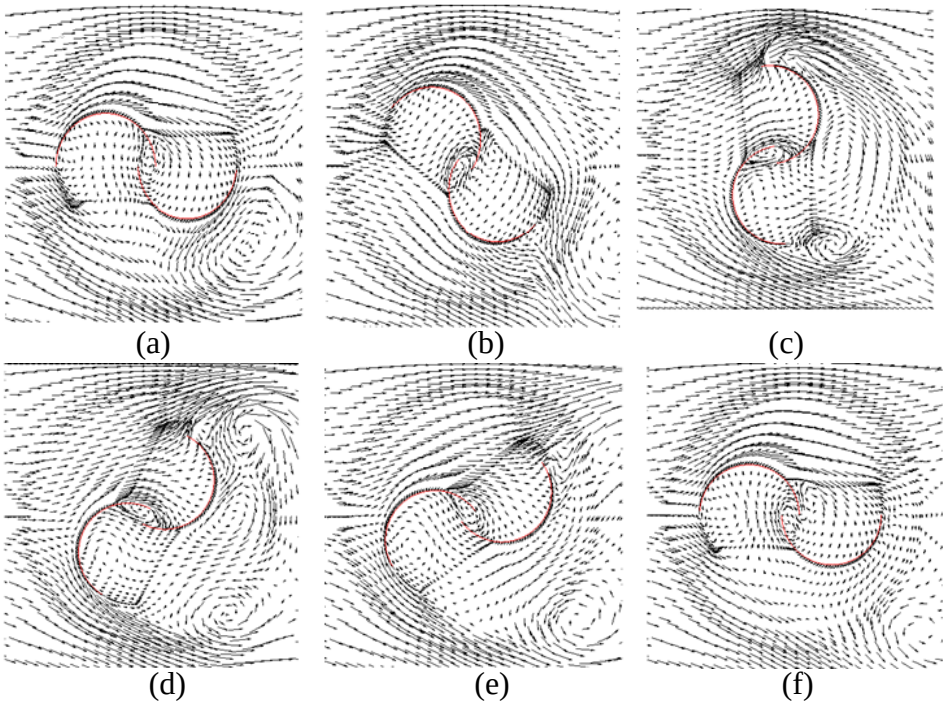

Figure 5: Velocity field near the blade of the lower rotating device
(angle of attack 0 degrees: flow from left to right)

Next, the flow field when the angle of attack is 0 degrees, 45 degrees, and 90 degrees is indicated by the velocity vector and the isobaric line in the region including the two devices for various rotation angles during the half rotation of the wind turbine. Fig.6 and 7 have an angle of attack of 0, 45 and 90 degrees. It can be seen that there was no unnaturalness at the boundary of each small region in each isobar even though the region was divided into small parts and the calculation was performed without problems in passing data between the regions.

In Fig.6 and 7 where the angle of attack is 0 degrees, it can be seen that the flow is almost vertically symmetrical.

Further, focusing on the portion sandwiched between the two rotating devices in Fig.6, it can be seen that the fluid is pushed out from left to right as the rotating device rotates, especially from (b) to (e). When the angle of attack is 45 degrees (Fig.8 and 9), the vertical symmetry of the flow is broken. Although not as strong as in Fig.6, fluid extrusion can be seen in the part sandwiched between the two rotating devices. A closer look reveals that the flow away from the lower leeward rotating device hits the leeward side device. When the angle of attack is 90 degrees (Fig.10 and 11), it can be seen that the leeward rotating device is contained in the wake portion created by the leeward rotating device. That is, it can be seen that only a weak flow hits the leeward rotating device.

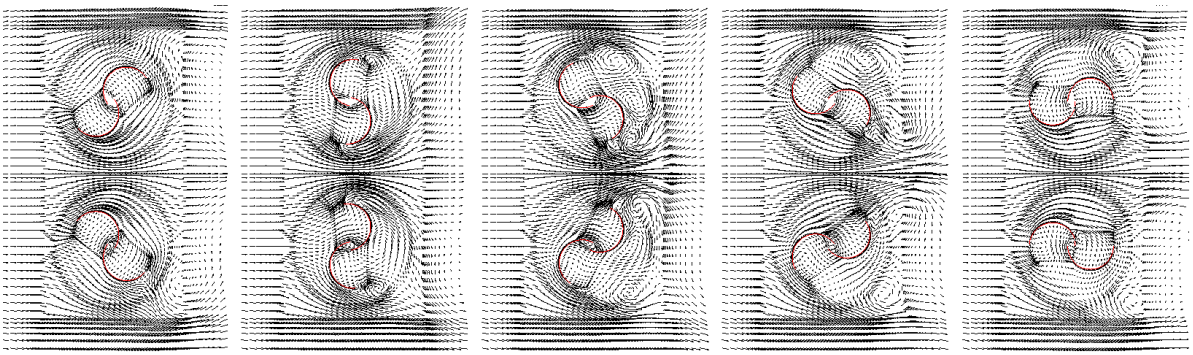

Figure 6: Flow field (velocity vector) near the two rotating devices when the angle of attack is 0 degrees (flow is from left to right)

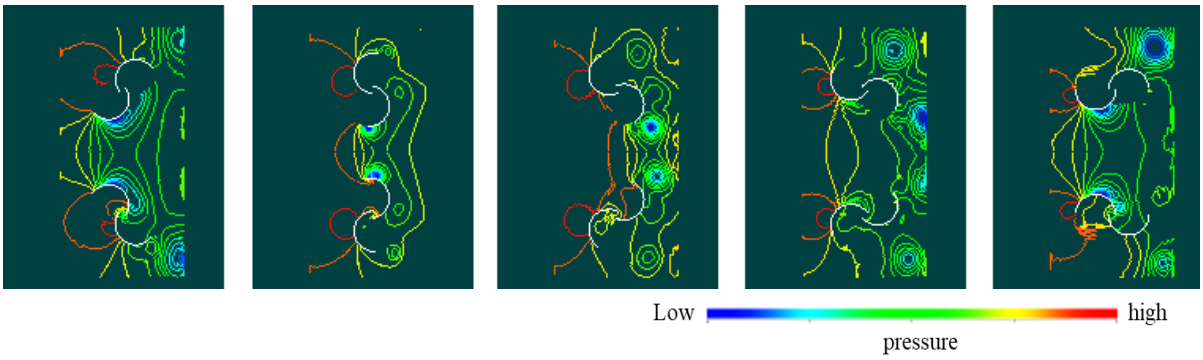

Figure 7: Flow field (isobar) near the two rotating devices when the angle of attack is 0 degrees (flow is from left to right)

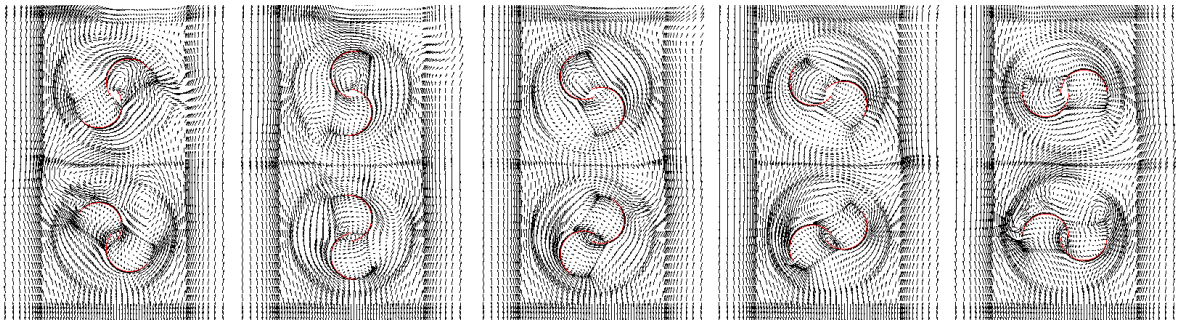

(a) (b) (c) (d) (e)

Figure 8: Flow field (velocity vector) near the two rotating devices when the angle of attack is 45 degrees (flow is from left to right)

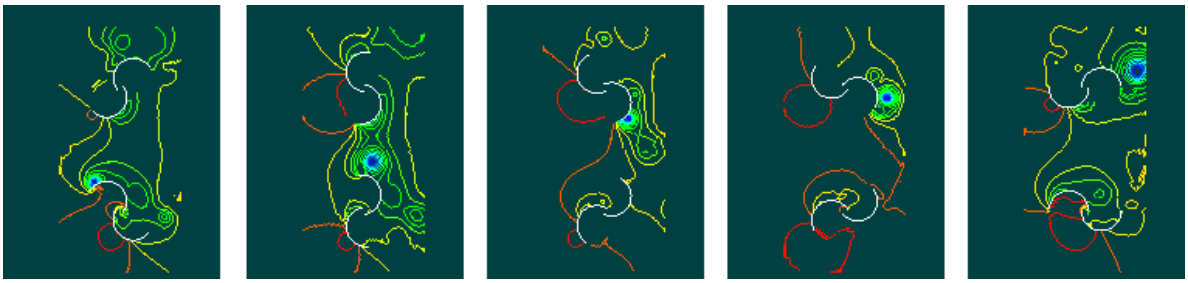

Figure 9: Flow field (isobar) near the two rotating devices when the angle of attack is 45 degrees (flow is from left to right)

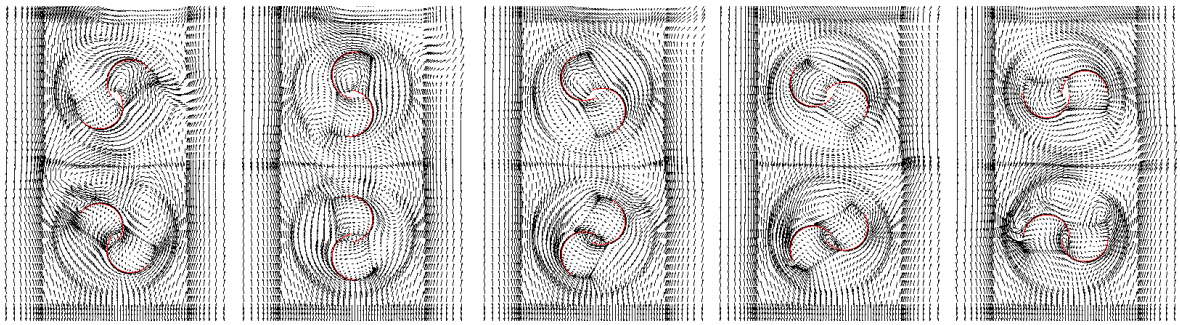

(a) (b) (c) (d) (e)

Figure 10: Flow field (velocity vector) near the two rotating devices when the angle of attack is 90 degrees (flow is from left to right)

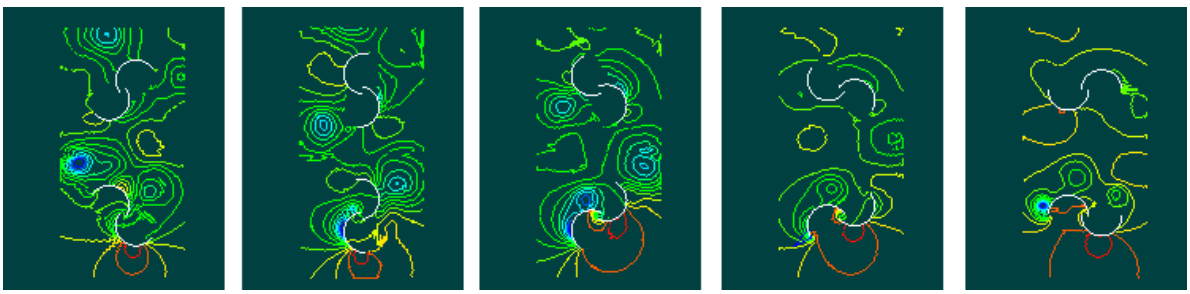

Figure 11: Flow field (isobar) near the two rotating devices when the angle of attack is 90 degrees (flow is from left to right)

3.2 Torque coefficient

Since the pressure acting on the surface of the blade can be obtained from the calculation result of the flow, the torque acting on the rotating device can be calculated using it. In reality, tangential stress also needs to be considered, but it is much smaller than that due to pressure and is ignored in this report. Fig.12 is a diagram plotting the torque acting on the two blades of the lower rotating device with respect to the rotation angle when the angle of attack is 0 degrees. It can be seen that the values are almost equal for the two blades and the phase is 180 degrees out of phase with the shape of the rotating device.

Fig.13 is a diagram showing how the torque of the lower rotating device (the sum of the torques of the two blades) changes depending on the rotation angle when the angle of attack is 0 degrees. For reference, the torque acting on the blade 1 (the one that was initially on the left) is also shown in the same figure. Here, the rotation angle 0 represents an initial state in which the line connecting the tips of the two blades is parallel to the flow. This initial arrangement is the same regardless of whether the angle of attack is 45 degrees or 90 degrees (for example, in the case of an angle of attack of 90 degrees, the flow is initially perpendicular to this arrangement). Since the torque acting on the upper rotating device is almost the same as the torque acting on the lower rotating device, it is not plotted in the figure.

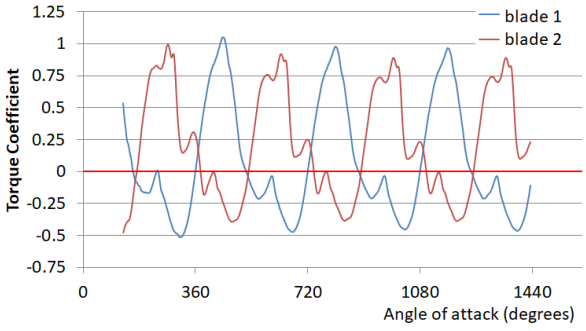

Figure 12: Torque acting on the two blades of the lower rotating device when the angle of attack is 0 degrees

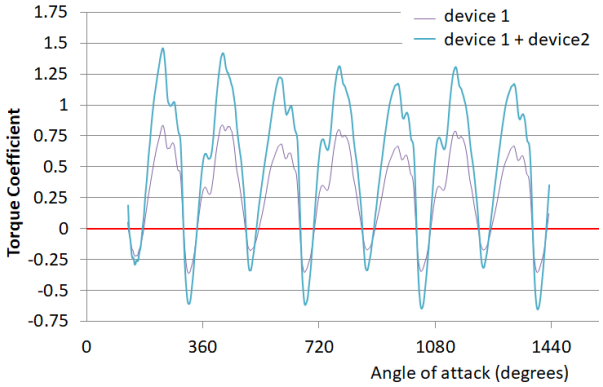

Figure 13: The rotation angle dependence of the torque acting on one blade and the total value of the two blades when the angle of attack is 0 degrees

Fig.14 is a diagram corresponding to Fig.13 when the angle of attack is 45 degrees. There are two types of curves because the two rotating devices are plotted separately, and the one with the larger instantaneous value is on the leeward side. It is considered that the phase shift between the windward side and the leeward side is the result of the interaction. Fig.15 is a diagram corresponding to Fig.14 the angle of attack is 90 degrees. The smaller value is on the leeward side, and in this case, there is a clear difference between the leeward side and the leeward side.

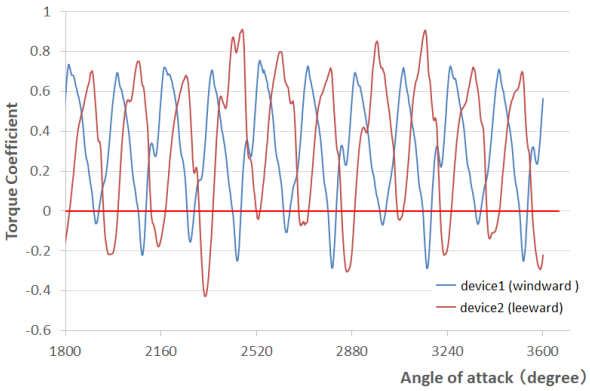

Figure 14: The rotation angle dependence of the torque acting on one blade and the total value of the two blades when the angle of attack is 45 degrees

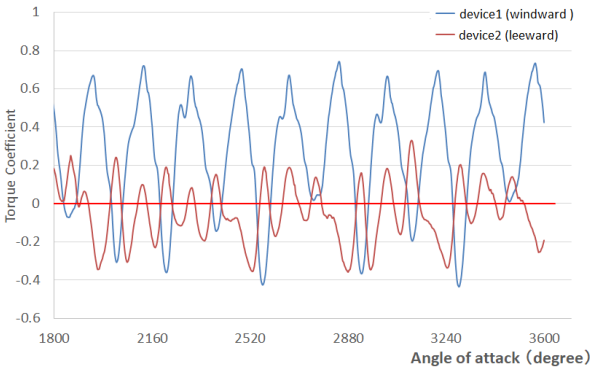

Figure 15: The rotation angle dependence of the torque acting on one blade and the total value of the two blades when the angle of attack is 90 degrees.

Fig.16 is an integrated value of the torque values of the two rotating devices based on the angle of rotation. In the case of 90 degrees, the integrated value is clearly small and less than half of the case of 0 degrees or 45 degrees. As for 0 degrees and 45 degrees, 0 degrees is larger while the angle is small, but it reverses around 1400 degrees (4 rotations), and 45 degrees is larger. It is probable that the reason is that the flow away from the leeward rotating device was strengthened by combining with the original flow and hit the leeward rotating device. In the case of 90 degrees, it is probable that the rotating device on the leeward side entered the wake of the leeward side and the flow was not effective for rotation.

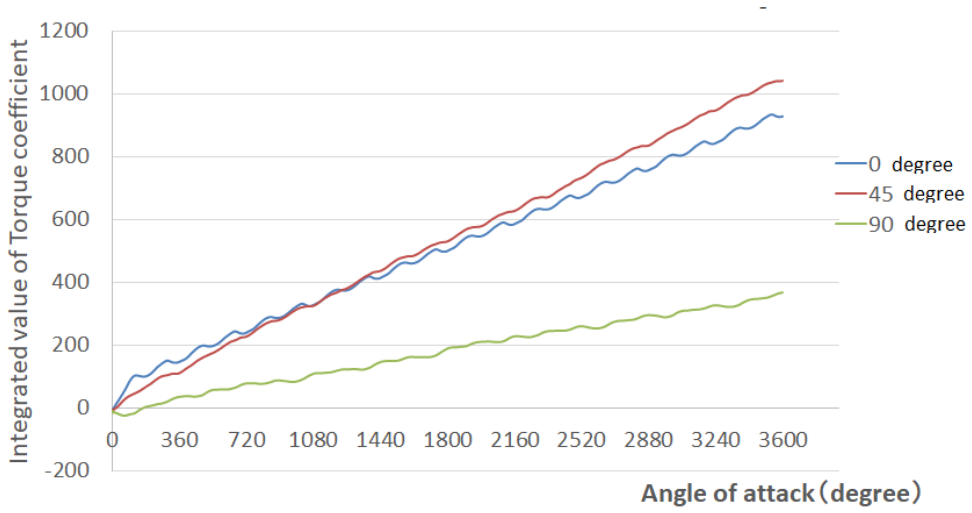

Figure 16: Integrated value of torque with respect to rotation angle (angle of attack: 0,45,90 degrees)

3.3 Effect of tip speed ratio

Fig.17 is a diagram in which the peripheral tip ratio is on the horizontal axis and the power coefficient is on the vertical axis, and the flow is 0 degrees, 45 degrees, and 90 degrees. The three cases of are drawn in the same figure. The power coefficient is large when the tip speed ratio is 45 degrees. It can be seen that the power coefficient takes the maximum value when the tip speed ratio is about 0.6 in the case of 45 degrees and when it is 0.7 in the case of 0 degrees. Furthermore, both of them have a negative value when it exceeds 1.2, indicating that the turbine does not rotate. In the case of 90 degrees, the power coefficient is considerably low, and when the tip speed ratio exceeds 0.8, it becomes a negative value.

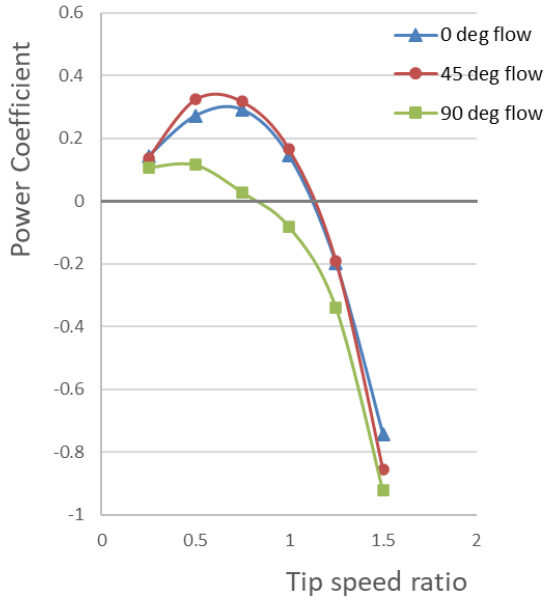

Figure 17: Dependence of power coefficient on tip speed ratio (angle of attack: 0,45,90 degrees)

4 SUMMARY

In this report, we performed a two-dimensional simulation of two vertical-axis Savonius-type rotating devices that rotate in the opposite direction, and investigated the effect of the interaction by changing the angle between them and the tip speed ratio. At that time, a method was used in which the flow region was divided into a proximity region of each rotating device and an external region that did not rotate, and the joints were connected with high accuracy. Moreover by dividing the inside of the Savonius type rotating device into a blade area and an overlapping area, it is possible to analyze the flow passing through the overlapping gap.

When the direction of the main flow was changed, it was observed that a complicated flow was generated due to the positional relationship between the two rotating devices. Almost the same torque was obtained at 0 degrees and 45 degrees, while the torque value at 90 degrees was smaller than that at 0 degrees and 45 degrees. The power coefficient took the maximum

value when the tip speed ratio was about 0.6 in the case of 45 degrees and when it was 0.7 in the case of 0 degrees.

The following issues can be raised as future ones:

The result was that the integrated value of the total torque of the two devices increased almost linearly with rotation, and it was found that stable output could be obtained with the two devices. From this, further calculations are needed by increasing the number of devices and consider the layout of the entire ocean current power generation system.

This time, the calculation was performed with the distance between two turbines fixed, and the interaction and the change in power were investigated. Therefore investigating the interaction and the power when the distance between two turbines is changed, and examining the conditions for obtaining the maximum power.

REFERENCES

[1] A. Henami, “Wind turbine technology” , Delmar Pub (2011)

[2] I. Paraschivoiu, “Wind Turbine Design: With Emphasis on Darrieus Concept” Polytechnic International Press (2002)

[3] T.Kawamura, Y.Sato, A.Shinohara and M. Kan: “Numerical Study of the Flow and Dynamics around a Cross-Flow Turbine”, Theoretical and Applied Mechanics Vol.51, pp.231-240(2002)

[4] Yuka Yoshida and Tetuya KAWAMURA, “Numerical simulation of flow around S-shaped rotor with slits on the blade”, Natural Science Report of the Ochanomizu University, 64(1), 2013, pp.1-12

[5] Miho ARAKI, Anna KUWANA and Tetuya KAWAMURA, “Numerical simulation on interaction of multiple S-shaped turbines”, Theoretical and Applied Mechanics Japan, Volume 64, pp.67-72 (2018).

[6] Yanenko, N. N., “ The method of fractional steps ”, Springer Springer-Velag, (1971)

[7] T. Kawamura and K. Kuwahara, “Computation of high Reynolds number flow around a circular cylinder with surface roughness” , AIAA Paper, 84 84-0340 (1984)